Asia-Pacific Journal of Atmospheric Sciences (2019) 55:75–89
https://doi.org/10.1007/s13143-018-0091-2

Online ISSN 1976-7951
Print ISSN 1976-7633

ORIGINAL ARTICLE

Combined Effect of the Madden-Julian Oscillation and Arctic Oscillation on Cold Temperature Over Asia

Hyun-Ju Lee[1] · Kyong-Hwan Seo[1] · Qigang Wu[2] · Seoung-Soo Lee[3] · Hyo-Seok Park[4]

Received: 31 May 2018 / Revised: 29 October 2018 / Accepted: 2 November 2018 / Published online: 9 November 2018

Abstract

The combined effect of the Madden–Julian oscillation (MJO) and Arctic oscillation (AO) on the temperature variation over Asia is investigated using the thermodynamic budget equation. Because of the distinct geographical origin of the two atmospheric modes, the influence of AO is more dominant in the higher latitude, whereas the MJO impact is more predominant in the lower latitude. Hence, the physical process responsible for the surface cold anomaly is different for northern and southern Asia. Cold anomaly appears in most of Asia 20–25 days after the MJO phase 6 (corresponding to the phase 2–3). However, more strengthened cold anomaly occurs over northern Asia under the negative AO state and it is caused by advection of temperature anomaly by climatological northerly wind associated with the East Asia winter monsoon flow. On the other hand, much stronger cold anomaly is seen over southern Asia under the positive AO state for the same lag day of the initial MJO phase 6. Aside from the upward overturning circulation forced by the tropical MJO over the subtropics and lower midlatitudes, the weakening of the East Asia subtropical jet by the positive AO induces additional upward motion over southern Asia to adjust the thermal wind balance. The combined effect of the MJO and AO also influences on the occurrence of extreme cold event. Under the negative (positive) AO phase, the extreme cold event occurrence probability over northern (southern) Asia increases by 90% (60%) compared to that for all winter days. The relative increase rate for the MJO phases 2–3 is ~30% over southern Asia. The cold event occurrence probability for the combined modes is about the twice that for only MJO impact, suggesting that an incorporation of both modes enhance the predictability of extreme cold event.

Keywords The madden-Julian oscillation · The Arctic oscillation · Extreme cold event · Combined effect · Thermodynamic budget equation

1 Introduction

The Madden-Julian oscillation (MJO) is the predominant physical mode in the tropics on the intraseasonal time scale of 30–70 days (Madden and Julian 1972). The MJO affects a variety of weather and climate phenomena and variables, including the surface temperature and circulations over East Asia (EA, Vecchi and Bond 2004; Seo et al. 2016), North America (Lin and Brunet 2009; Zhou et al. 2012; Seo and Son 2012; Seo et al. 2016; Seo and Lee 2017) and the Arctic region (Yoo et al. 2012), and precipitation in EA (Jeong et al. 2008) and Canada (Lin et al. 2010). It also influences the Asian and Australian monsoon (Hendon and Liebmann 1990; Hoyos and Webster 2007) and tropical cyclones (Hall et al. 2001; Bessafi and Wheeler 2006; Kim and Seo 2016). In particular, the MJO is mainly responsible for the

Responsible Editor: Sang-Wook Yeh.

✉ Kyong-Hwan Seo
khseo@pusan.ac.kr

[1] Department of Atmospheric Sciences, Division of Earth Environmental System, Pusan National University, Busan, South Korea

[2] Department of Atmospheric and Oceanic Sciences, Institute of Atmospheric Sciences, Fudan University, Shanghai, China

[3] Earth System Science Interdisciplinary Center (ESSIC), University of Maryland, College Park, MD, USA

[4] Korea Institute of Geoscience and Mineral Resources, Daejeon, South Korea

intraseasonal temperature variation over EA because of the proximity of forcing center to this region (Seo et al. 2016). For instance, when enhanced (suppressed) convection is located over the Indian Ocean (western Pacific) at around the MJO phase 2–3, warm anomaly develops over EA during the next 10 to 20 days. The major factor for this is analyzed to be the adiabatic upward motion that comes from the tropics and subsidence warming over EA by the MJO-induced local overturning circulation. The horizontal advection by the MJO-induced horizontal advection and radiative effects may also play a role in temperature changes (Jeong et al. 2005).

Recently, a few studies have examined a combined impact of the MJO with other atmospheric modes that have the longer time scale such as the El Niño–Southern Oscillation (ENSO) (Moon et al. 2011; Shimizu and Ambrizzi 2016), quasi-biennial oscillation (QBO) (Liu et al. 2014; Marshall et al. 2017) and Arctic oscillation (AO) (Park et al. 2010). For example, Park et al. (2010) have investigated cold surges over Korea by taking account of both the MJO and AO. The AO is the tropospheric variability related to a fluctuation of the polar vortex, which is strongly associated with the surface temperature over the northern Eurasian continent (Thompson and Wallace 1998). A blocking-type cold surge can be reinforced at the MJO phase 2–3 during the negative AO. This reinforcement is caused by a southward expansion of the Siberian high that is modulated by the AO and the upward motion that is induced by Rossby wave response to the MJO (Park et al. 2010). Since a combination of the influences of two oscillations produces enhanced or cancelling responses over EA, it is crucial to investigate both factors together. However, detailed processes are not fully resolved. In particular, a relative importance among the related processes needs to be explicitly evaluated using a governing equation. Although Park et al. (2010) have examined the impacts of the MJO and AO on cold surges, the focused area is limited to Korea and they have analyzed cold surge through a case study with one year. In general, the AO affects higher latitudes and midlatitudes, and the MJO influences the subtropical region or lower midlatitudes. Hence, their combined impact areas can be different depending on a relative dominance of each impact. So in this study, to investigate a detailed physical mechanism, Asia is divided into two regions: northern Asia, [100° − 140°E, 40° − 55°N], and southern Asia, [60° − 120°E, 25° − 40°N].

In this study, the surface temperature variation over Asia in response to the MJO is examined under different AO phase. Using a thermodynamic equation, the relative importance in the physical processes responsible for the temperature variation is unveiled. In addition, the occurrence probability of extreme cold event is calculated using a gridded station dataset. The present study investigates whether incorporation of the MJO and AO produces extreme cold event more frequently. Therefore, this information can help improve the predictability of extreme weather events. Section 2 contains the description of the data and methods and in Section 3, two domains are selected and related predominant physical mechanisms are investigated. The occurrence percentage of extreme cold event is also examined in Section 3. The summary and discussion is presented in Section 4.

2 Data and Methods

The dataset is obtained from the Japanese 55-year reanalysis project (JRA-55) of the Japan Meteorological Agency (JMA) for the period from 1979 to 2010 (Kobayashi et al. 2015). The variables used are 2-m temperature, air temperature, geopotential height, horizontal and vertical wind, and total diabatic heating rate. To identify the tropical deep convection, the Advanced Very High-Resolution Radiometer (AVHRR) outgoing longwave radiation (OLR) daily mean data from the National Oceanic and Atmospheric Administration (NOAA) is used. The first three harmonics of the annual cycle for variables are subtracted to obtain the anomaly. To categorize the eight MJO phases, the empirical orthogonal function (EOF) analysis is performed with the 20–90-day bandpass-filtered OLR. A phase is defined by the first two leading principal components (PC1 and PC2) and the amplitude is calculated as $\sqrt{PC1^2 + PC2^2}$ (Wheeler and Hendon 2004). The phase 2–3 indicates enhanced (suppressed) convection being located over the Indian Ocean (western Pacific) and the phase 4–5 represents the period when enhanced (suppressed) convection is located over the Maritime continent (the central Pacific). The AO index is obtained from the National Weather Service Climate Prediction Center (http://www.cpc.ncep.noaa.gov/products/precip/CWlink/daily_ao_index/ao_index.html). In this study, the DJF (December to February)-mean AO index is used for selecting strong or weak AO winters.

To identify the individual influence of the MJO and AO on temperature variation, a composite analysis is performed for days when the MJO amplitude is greater than 0.43 standard deviations (equivalent to the upper 33% of the total probability) and for winters when DJF-mean AO index is greater (smaller) than 0.50 (−0.50) standard deviations. For the sake of simplicity, for example, the composite for the MJO phase 1 is referred to as 'MJOp1' hereafter. Similarly, the composites of the negative and positive AO are referred to as 'AO^-' and 'AO^+', respectively. To investigate the combined effect, winters with the AO index being greater (smaller) than 0.50 (−0.50) standard deviations are extracted for the positive (negative) AO, and then, only days when the MJO index is greater than 0.43 standard deviations are selected among the extracted winters. For lagged composite, if the days exceed a period of DJF, the case is excluded. Accordingly, the composite for the MJO phase 1 under the negative and positive AO states are referred to as '$MJOp1|AO^+$' and '$MJOp1|AO^-$',

Table 1 List of the number of selected days for each of eight MJO phases. The number is for all winters, and for negative and positive AO winters

	1	2	3	4	5	6	7	8	Total
MJO (32 yrs)	182	238	223	218	184	233	256	239	1773
MJO| AO^- (9 yrs)	34	48	59	59	32	43	82	87	444
MJO|AO^+ (10 yrs)	83	65	60	77	74	78	77	68	582

respectively. In addition, 'MJOp2–3' ('MJOp6–7') indicates the composite for the MJO phases 2 and 3 (6 and 7). The numbers of selected winter and day are presented in Table 1. The result is not sensitive to the choice of a threshold value.

To determine the occurrence probability of extreme cold event depending on the MJO phases and AO states, the gridded global station data from the Hadley Centre Global Historical Climatology Network−Daily (HadGHCND) dataset is used. The extreme cold event is defined as days when temperature is lower than −1.645 standard deviations, which accounts for the upper 5% cold events. So the occurrence probability of extreme cold event is calculated as a ratio of the number of the top 5% events to the number of total selected days. A Monte-Carlo test based on 500 random samples is applied for the evaluation of a statistical significance of the composites and occurrence probability of extreme cold event.

The thermodynamic equation used here is as follows (Seo et al. 2016):

$$\frac{\partial T'}{\partial t} = -\overline{\overrightarrow{V_H}}\cdot\nabla_H T' - \overrightarrow{V_H}'\cdot\nabla_H \overline{T} - \left(\overrightarrow{V_H}'\cdot\nabla_H T' - \overline{\overrightarrow{V_H}'\cdot\nabla_H T'}\right) + \left(\frac{R}{C_P}\frac{T'}{p} - \frac{\partial T'}{\partial p}\right)\overline{\omega} + \left(\frac{R}{C_P}\frac{\overline{T}}{p} - \frac{\partial \overline{T}}{\partial p}\right)\omega' + \left\{\left(\frac{R}{C_P}\frac{T'}{p}\omega' - \frac{\partial T'}{\partial p}\omega'\right) - \overline{\left(\frac{R}{C_P}\frac{T'}{p}\omega' - \frac{\partial T'}{\partial p}\omega'\right)}\right\} + Q_{Dia}' + Res'. \quad (1)$$

Here, T, $\overrightarrow{V_H}$ and ω are the temperature, horizontal velocity and vertical velocity in pressure coordinates, respectively. p is the pressure, C_P is the specific heat of dry air at constant pressure, and R is the gas constant for dry air. Q_{Dia} is the total diabatic heating rate and *Res* indicates a residual term including the diffusion and numerical error. Overbar represents the climatology and prime is the anomaly, respectively. In Eq. (1), the left-hand term is the temperature anomaly tendency. The first four terms on the right-hand side are the temperature advection by the horizontal wind with each representing the anomalous temperature advection due to the climatological horizontal wind, climatological temperature advection by the horizontal wind anomaly, and nonlinear advection terms between anomalies. The next four terms are related to the adiabatic heating process: the interaction between the temperature anomaly and climatological vertical velocity, interaction between the climatological temperature and vertical velocity anomaly, and nonlinear adiabatic terms between anomalies. A sum of the horizontal temperature advection and adiabatic terms is denoted as the dynamic term. The ninth term represents the anomaly of the total diabatic heating rate, and the last term is residual term (which is relatively small so it is neglected).

Additionally, each of terms in Eq. (1) is integrated with respect to lag days as a following form (Seo et al. 2016):

$$\int_{lag=0}^{lag=t} \frac{\partial A}{\partial t}\,dt = A(t), \quad (2)$$

where A is each of the individual terms in Eq. (1). Through the transformation, a unit of each term is modified from K day^{-1} into K. Then, the outcome represents an accumulated temperature change from day 0 to day t.

3 Response of Temperature and Circulation to the AO and MJO

Prior to the investigation of the combined effect of the MJO and AO, each influence on the temperature variation over Asia is identified. Figures 1a, b show the composites for the negative and positive AO winters, respectively. A robust and widespread negative temperature anomaly is seen over the northern Eurasian continent at the negative AO winter, but it is confined to the north of 45°N (Fig. 1a). The cold anomaly flows down from the polar region into northeastern Asia. The center of the upper-level trough (green contour in Fig. 1a) is located to the west of the lower-level trough (black contour in Fig. 1a), indicating a developing baroclinic system (Holton 2004). Hence, below the center of the upper-level trough, a decrease in thickness (Fig. 1a) is expected to develop and therefore strong cold advection appears (Wu and Chan 1997; Jeong and Ho 2005). Meanwhile, a weak positive temperature anomaly lies in inland China, suggesting that it is too far for the cold anomaly to reach the region. Similarly, but with an opposite sign, for the positive AO winter (Fig. 1b), a strong warm anomaly develops in the high latitudes and relatively weak cold anomaly in the lower midlatitudes. On the other hand, the MJO phases 2–3 (6–7) (Figs. 1c, d) produces extensive cold (warm) temperature and negative (positive) geopotential height anomalies in most of the Eurasian continent. A cause of the temperature variation in the southern part of the Eurasian continent has been identified as the MJO-induced adiabatic process (Seo et al. 2016). However, a process inducing the temperature variation in the northern part of the Eurasian continent is not understood yet. Because the East Asian subtropical jet disturbs a northward propagation of the Rossby wave response to the MJO, it

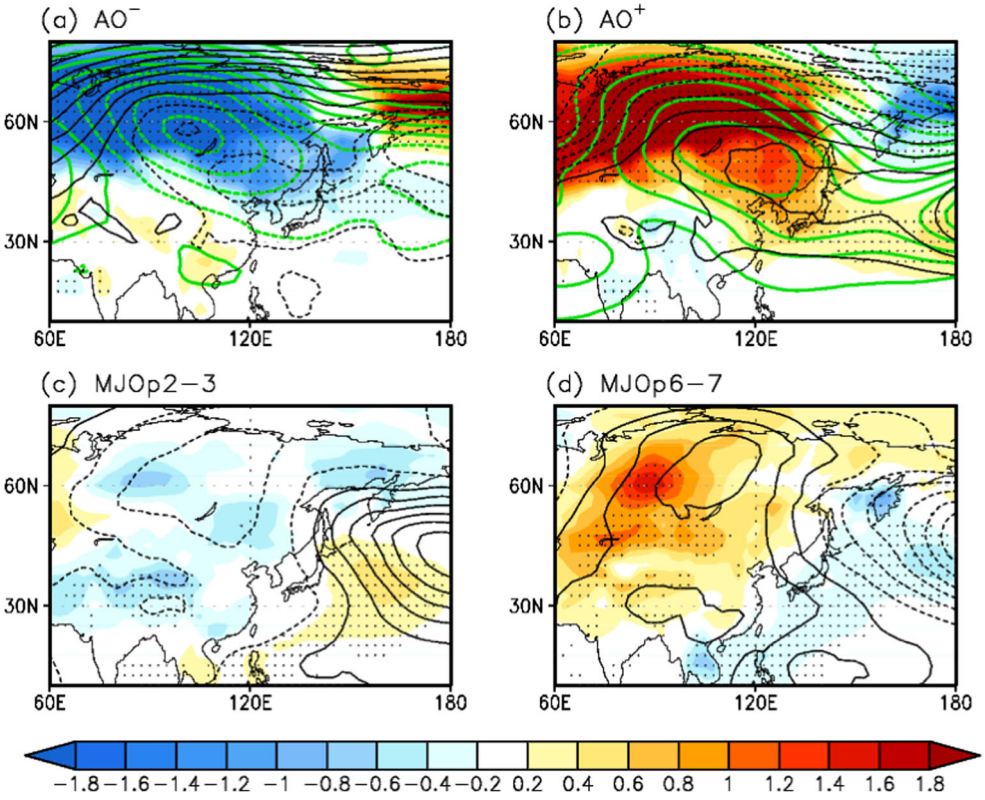

Fig. 1 Composite maps of 300-hPa (green contour; intervals of 10 gpm) and 850-hPa (black contour; intervals of 5 gpm) geopotential height and 2-m temperature (shaded; K) anomalies for (**a**) AO^- and (**b**) AO^+ winters. Composite maps of 850-hPa geopotential height (black contour; intervals of 5 gpm) and 2-m temperature (shaded; K) anomalies for (**c**) MJO phase 2–3 and (d) phase 6–7. Note that the composites with respect to the AO and MJO are calculated with winter-mean and daily fields, respectively. Dots indicate statistically significant areas of temperature field at the 95% confidence level

is hard to explain the physical mechanism (Branstator 2002; Adames and Wallace 2014).

Figure 2 is the composites of the temperature anomaly at the MJO phase 2–3 during each AO state. Hereafter, only cold anomalies are focused since it can bring about the extreme weather and climate events during wintertime. So, the case for the MJO phase 6–7 under the AO state is omitted. At the negative AO, the temperature pattern is typically manifested with an enhanced cold anomaly over the northern Eurasian continent (Fig. 2a), while for the positive AO winter (Fig. 2b), an intense cold anomaly appears over the southern Eurasian continent. This suggests that a combination of the two types of variability generates a much stronger cold anomaly over Asia. Furthermore, it is obvious that distinct processes operate in the different regions of Asia. Therefore, two regions (i.e., northern Asia and southern Asia) are separately examined.

4 Related Physical Mechanisms

4.1 Northern Asia

To show an evolution of the temperature change over northern Asia, the lagged composite for the MJO phase 6 is presented in Fig. 3. Given that the time interval

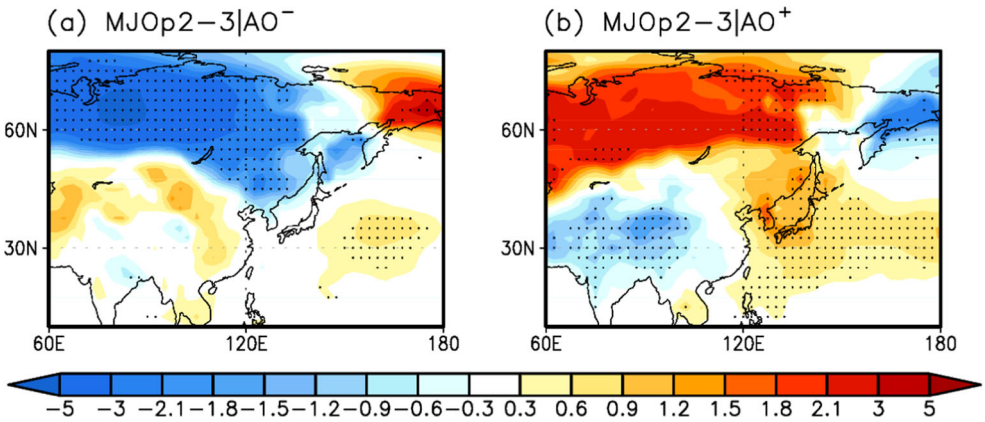

Fig. 2 Composite maps of 2-m temperature anomaly in daily fields for the MJO phase 2–3 during (**a**) AO^+ and (**b**) AO^- winters. The unit of temperature anomaly is K. Dots are statistically significant areas at the 95% confidence level

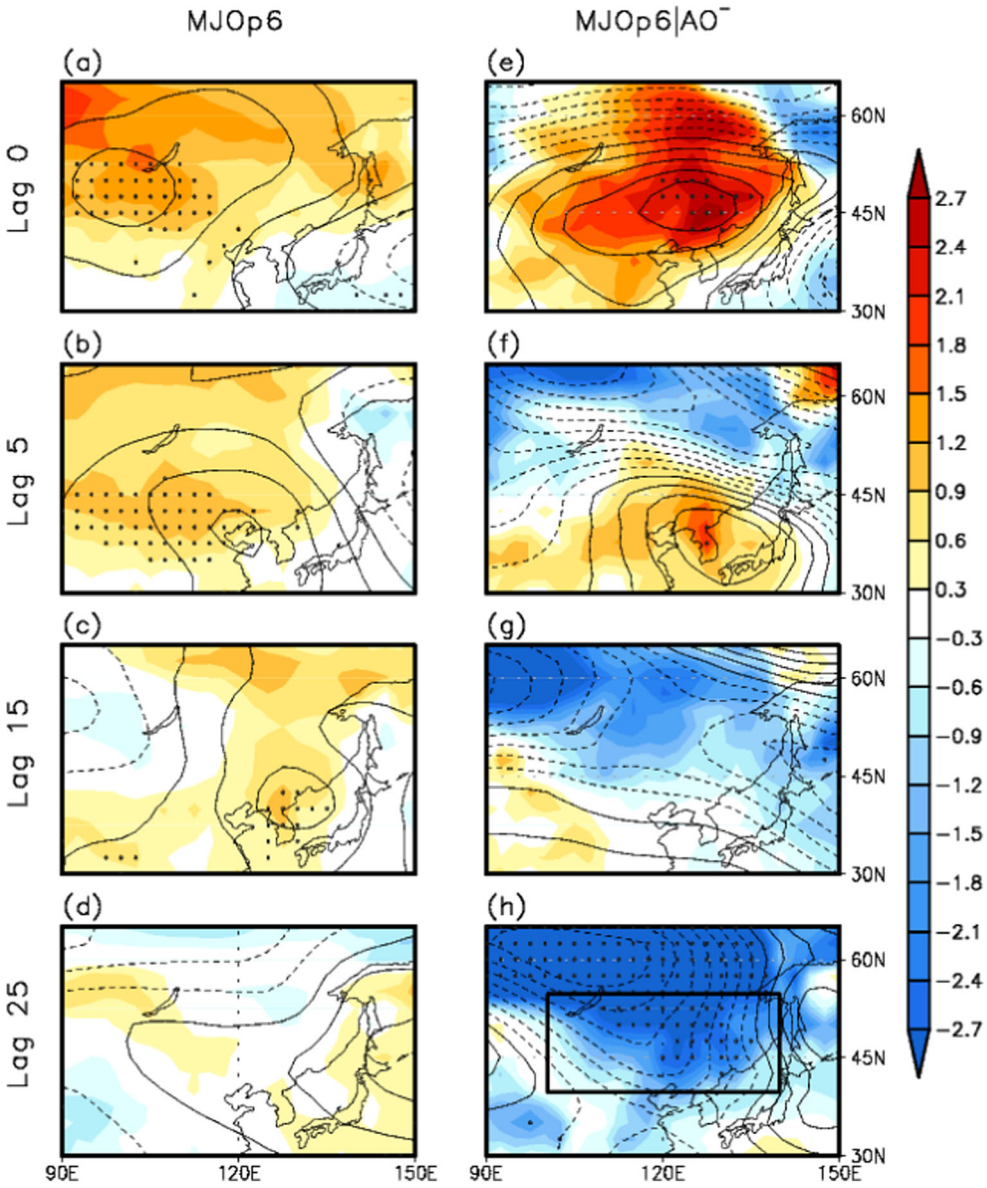

Fig. 3 Lagged composite maps of 500-hPa geopotential height (contour; intervals of 10 gpm) and 2-m temperature (shaded; K) anomalies at days 0, 5, 15, and 25 for (**a**) − (**d**) MJO phase 6 during all winters and (**e**) − (**h**) MJO phase 6 during AO^- winter. Dots represent statistically significant areas of temperature field at the 95% confidence level. Black box indicates the northern Asia region, [100° − 140°E, 40° − 55°N]

between two MJO phases is approximately 5–6 days, days 20 to 25 after the phase 6 corresponds to the phases 2 and 3. The result shows the development of the warm temperature and positive geopotential height anomalies over northern Asia including southeastern Russia, Mongolia, and northeast China at day 0, suggestive of the warm air advection and radiative heating (Fig. 3a). The warm anomaly disappears with time and eventually there is no significant signal after 25 days (Figs. 3b, c and d). Under the negative AO state (Fig. 3e), the positive geopotential height anomaly appears over northern Asia at day 0. However, it is weakened within the next 10 days and the strong negative geopotential height anomaly covers the region with severe cold anomaly at day 25 (Figs. 3f, g and h). To investigate the related physical process, the time-height lagged composite is performed using Eqs. (1) and (2) for the northern Asia domain, which is defined as [100° − 140°E, 40° − 55°N]. The domain is represented as a black box in Fig. 3h.

Temporal evolutions of each term of the thermodynamic equation are plotted in Fig. 4. By comparing these terms quantitatively, the predominant physical mechanism can be assessed. For the composite of only the MJO influence (left panels), weakening of the warm anomaly after day 0 is demonstrated in the temperature and tendency terms (Figs. 4a, b). The cold anomaly near the surface (Fig. 4b) is attributed to the diabatic process (Fig. 4f) of the radiative cooling (not shown). The dynamic term denotes a warm anomaly near the surface (Fig. 4c), whereas the advective term induces the cold anomaly at the lower level (Fig. 4e). The adiabatic term presents a warm anomaly below 150 hPa, which indicates that the impact of the local overturning circulation cannot reach this

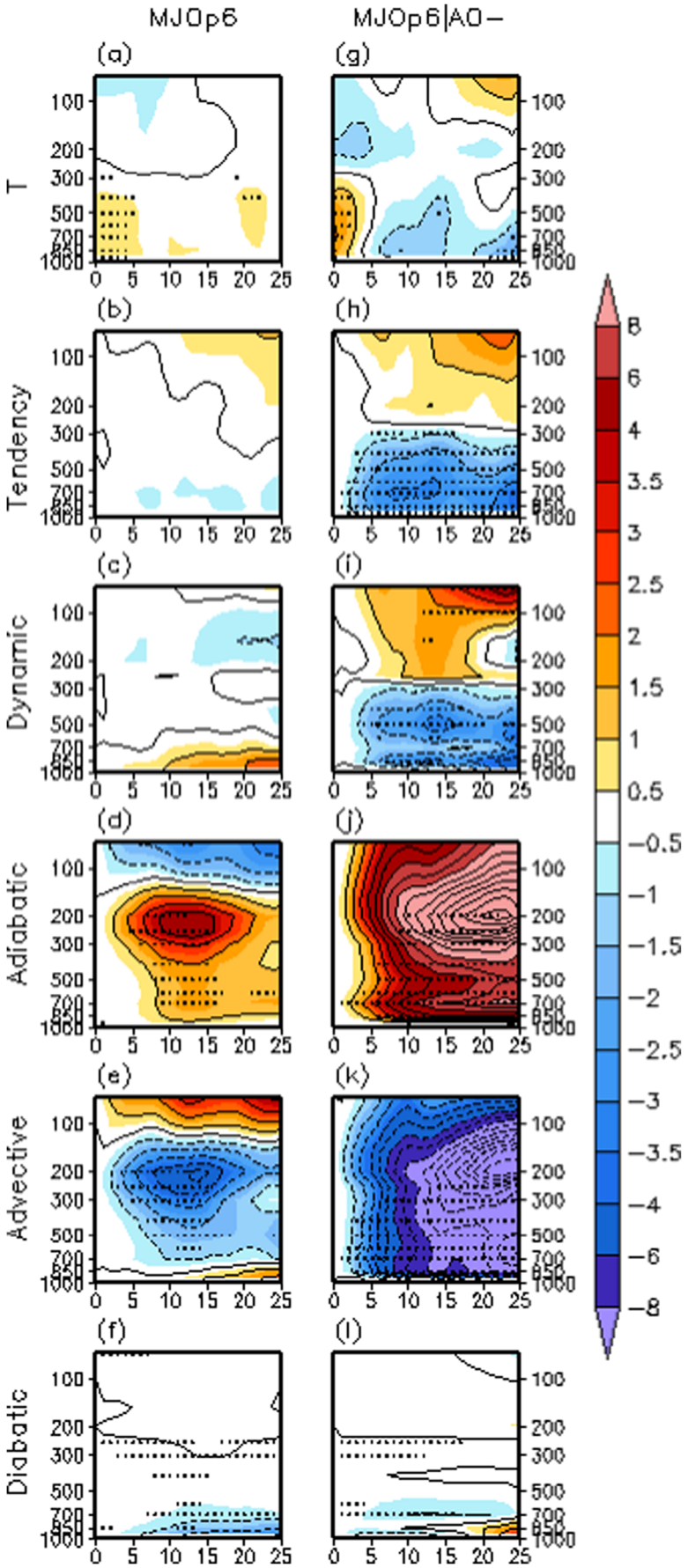
MJOp6
MJOp6|AO−
(a)
(g)
(b)
(h)
(c)
(i)
(d)
(j)
(e)
(k)
(f)
(l)
T
Tendency
Dynamic
Adiabatic
Advective
Diabatic
100
200
300
500
700
850
1000
0 5 10 15 20 25
8
6
4
3.5
3
2.5
2
1.5
1
0.5
−0.5
−1
−1.5
−2
−2.5
−3
−3.5
−4
−6
−8

◀ **Fig. 4** Time-height cross section of lagged composite of the temperature fields (units of K) over northern Asia for (**a**) – (**f**) the MJO phase 6 during all winters and (**g**) – (**l**) the MJO phase 6 during AO^- winter. From top to bottom: temperature anomaly, temporally integrated temperature fields from the tendency, dynamic, adiabatic, horizontal advective, and diabatic terms. The temperature below the surface is not plotted. Black dots indicate statistically significant areas at the 95% level

region because of a long distance from the origin (Fig. 4d). This is indirectly supported by examining the southern Asia area which is located more close to the tropics and over which cold anomaly is induced by adiabatic process through the overturning circulation (Fig. 7d, which will be described in next sub-section). In sum, the diabatic cooling due to a

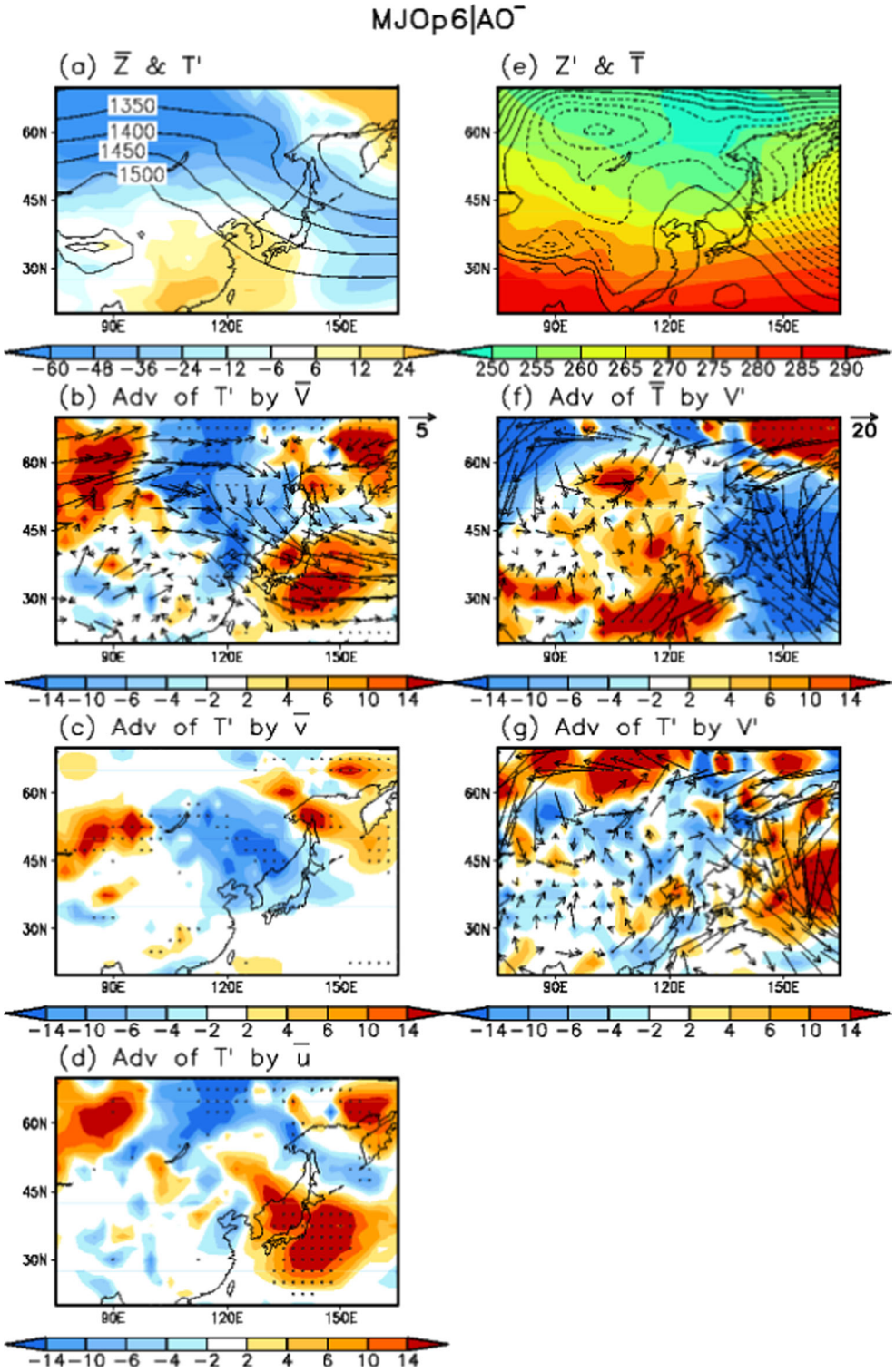

Fig. 5 Composite maps related to the horizontal temperature advection at 850 hPa. All anomalies are integrated with respect to 25 lag days for phase 6 during AO^- winter. (Left panels) Composite of (**a**) climatological geopotential height (contour; intervals of 50 gpm), air temperature anomaly (shaded; K day), (**b**) advection term (shaded; K) due to climatological horizontal wind (vector; m s^{-1} day), and (**c**) its meridional and (**d**) zonal components (shaded; K). (Right panels) Composite of (**e**) climatological air temperature (shaded; K), geopotential height anomaly (contour; intervals of 10 gpm day), (**f**) advection term (shaded; K) by horizontal wind anomaly (vector; m s^{-1} day), (**g**) nonlinear advection terms between anomalies (shaded; K), and horizontal wind anomaly (vector; m s^{-1} day). Dots in (b), (c), and (e) represent statistically significant areas of advection terms at the 95% confidence level

radiative process is mainly responsible for the surface cold anomaly and the cold advection also contributes to the cold anomaly at lower level. The latter is consistent with the result of Jeong et al. (2005). On the other hand, the composite under the negative AO state shows a rapid decrease of the temperature anomaly onward from day 0 (Fig. 4g). The cold anomaly is seen below 300 hPa with a minimum value of −2.2 K at the surface by day 25 (Fig. 4g). The tendency term (Fig. 4h) is almost identical to the dynamic term (Fig. 4i), which is nearly due to the advective cooling (Fig. 4k). The main contribution among the advection terms in Eq. (1) is the advection of the anomalous temperature due to the climatological horizontal wind (see Figs. 5a, b and c). The adiabatic term (Fig. 4j) shows an opposite effect to the advective term (Fig. 4k) and the diabatic term shows a warm anomaly at the surface after day 12 (Fig. 4l).

To demonstrate more detailed dynamics related to the horizontal advection, we divide each component of first two advection terms on the right-hand side of Eq. (1). All anomalous components are also integrated with respect to lag days of phase 6. Here, the geopotential height can be regarded as horizontal winds. The climatological geopotential height shows the East Asian winter monsoon over Siberia (contour in Fig. 5a). The climatological northwesterly wind (vector in Fig. 5b) is responsible for the advection of the cold temperature anomaly (shading in Fig. 5b) from Siberia to northern Asia. In particular, the meridional advection is more important (Fig. 5c) than the zonal advection (Fig. 5d). The preexisting cold anomaly over Siberia (shading in Fig. 5a) is caused by a southward expansion of cold air due to the weakening of the polar vortex at the negative AO (not shown). On the other hands, the advection of the climatological temperature by the wind anomaly shows a rather warm anomaly (shading in Fig. 5f). Because the lower-level geopotential height anomaly is located in inland China (contour in Fig. 5e), the southerly wind anomaly is induced along the east coast of China up to northern Asia (vector in Fig. 5f). This results in the warming in northern Asia. The nonlinear advection by anomalies (Fig. 5g) also contributes to the cold anomaly but it is relatively weak over northern Asia.

4.2 Southern Asia

To elucidate the enhanced cold anomaly over the southern Eurasian continent arising at the MJO phase 2–3 under the positive AO state, the lagged composite for the phase 6 is plotted in Fig. 6. The composite that considers the MJO impact shows a warm anomaly in the southern Eurasian continent up to day 15 (Figs. 6a, b and c). After that, the cold anomaly develops across the domain (Fig. 6d). Under the positive AO state, the geopotential height and temperature are seen to enhance over the southern Eurasian continent during 15 days (Figs. 6e, f and g). However, the situation is rapidly changed after day 15 (Fig. 6h), as the strong cold anomaly dominates in the region. To find the physical process responsible for the development of this cold anomaly, we define the southern Asia domain as [60° − 120°E, 25° − 40°N], which is marked by a black box in Fig. 6h. The domain includes southern EA, southeastern central Asia, and the area north of India, but excludes the Indian subcontinent and the Indochina peninsula.

Figure 7 is the time-height lagged composite for southern Asia. The composite incorporating the positive AO impact (right panels) is similar to that with no consideration of the AO effect (left panels), but the intensity in right panels is greater than that in left panels. In both composites, a decrease in the temperature appears below 400 hPa with time (Figs. 7a, b, g, and h) and the dynamic process (Figs. 7c, i) is responsible for the cold anomaly. The diabatic term (Figs. 7f, l), showing warm anomaly at the mid and lower troposphere, has an opposite effect to the dynamic effect. Among the dynamic processes, the adiabatic process is dominant (Figs. 7d, j) and it will be shown in Fig. 8 that this is mainly caused by an interaction between the climatological temperature and vertical wind anomaly. Meanwhile, the advective term shows a warm anomaly at all levels after about day 10 (Figs. 7e, k).

An interesting point in the above result is that the adiabatic cooling (Fig. 7j) is more strengthened under the positive AO phase. This can be explained in Figs. 8 and 9. The lagged composite of the zonal-averaged adiabatic term (i.e., interaction between the climatological temperature and anomalous vertical wind) (Fig. 8a) shows that a local overturning circulation develops in response to suppressed MJO convection over the tropical Indian Ocean, inducing an upward motion in the subtropics and lower midlatitudes at day 25. The ascent drives the adiabatic cooling over southern Asia. However, it should be noticed that this upward motion is much stronger under the positive AO state (Fig. 8b) than that for only MJO phase (Fig. 8a) and accordingly the cooling is stronger in the former state than in the latter composite. This can be attributed to the background field of the positive AO state (Fig. 9). During the positive AO phase, the polar vortex and midlatitude anticyclone are enhanced so polar jet (not shown) is strengthened, whereas the East Asian subtropical jet is weakened (blue shading in Fig. 9a). The weakening of the subtropical jet at the jet entrance reduces a vertical wind shear and disrupts a thermal wind balance. Consequently, an ageostrophic secondary circulation is generated to restore the thermal wind balance and therefore the divergence anomaly is induced near the jet entrance (thin solid contour in Fig. 9a). This anomalous divergence contributes to enhancement of the upward motion

over southern Asia (blue shading Fig. 9b). So, the stronger adiabatic cooling shown in Figs. 7j and 8b is due to the combined effects of upward motion anomaly which is formed by the AO-induced weakening of the subtropical jet, and overturning circulation anomaly which is forced by MJO suppressed convection.

5 Predictability of Extreme Cold Event

To determine whether the dynamic mechanism operates for the development of extreme cold event, a spatial distribution of the occurrence probability of extreme cold event (defined as the day with the surface temperature less than −1.645 standard deviations) is presented for the AO and MJO states (shading in Figs. 10 and 11). The criteria for distinguishing AO phase and MJO are ±0.50 and 0.43, respectively. At the negative AO state (Fig. 10a), the domain-averaged extreme cold event occurrence probability is ~ 10% in northern Asia, in particular, more than 14% in Siberia. At the positive AO phase (Fig. 10b), the probability averaged over the southern Asia domain is only 5% and statistically insignificant.

On the other hand, the occurrence probability at the MJO phase 2–3 is greater than phase 6–7 (Figs. 10c, d). The percentage for phase 2–3 (Fig. 10c) is more than 8.9% over central China, [107.5°E, 37.5°N], and 6.7% near northeast China, [120°E, 52.5°N] (the domain-averaged probability is 5–6% for southern Asia and northern Asia). For the purpose of the practical prediction for cold temperature event, the lagged plot of the occurrence probability is helpful. Figure 11 shows this probability for lag days after the peak of the MJO phase 6 (shading in Fig. 11). Without considering the AO influence

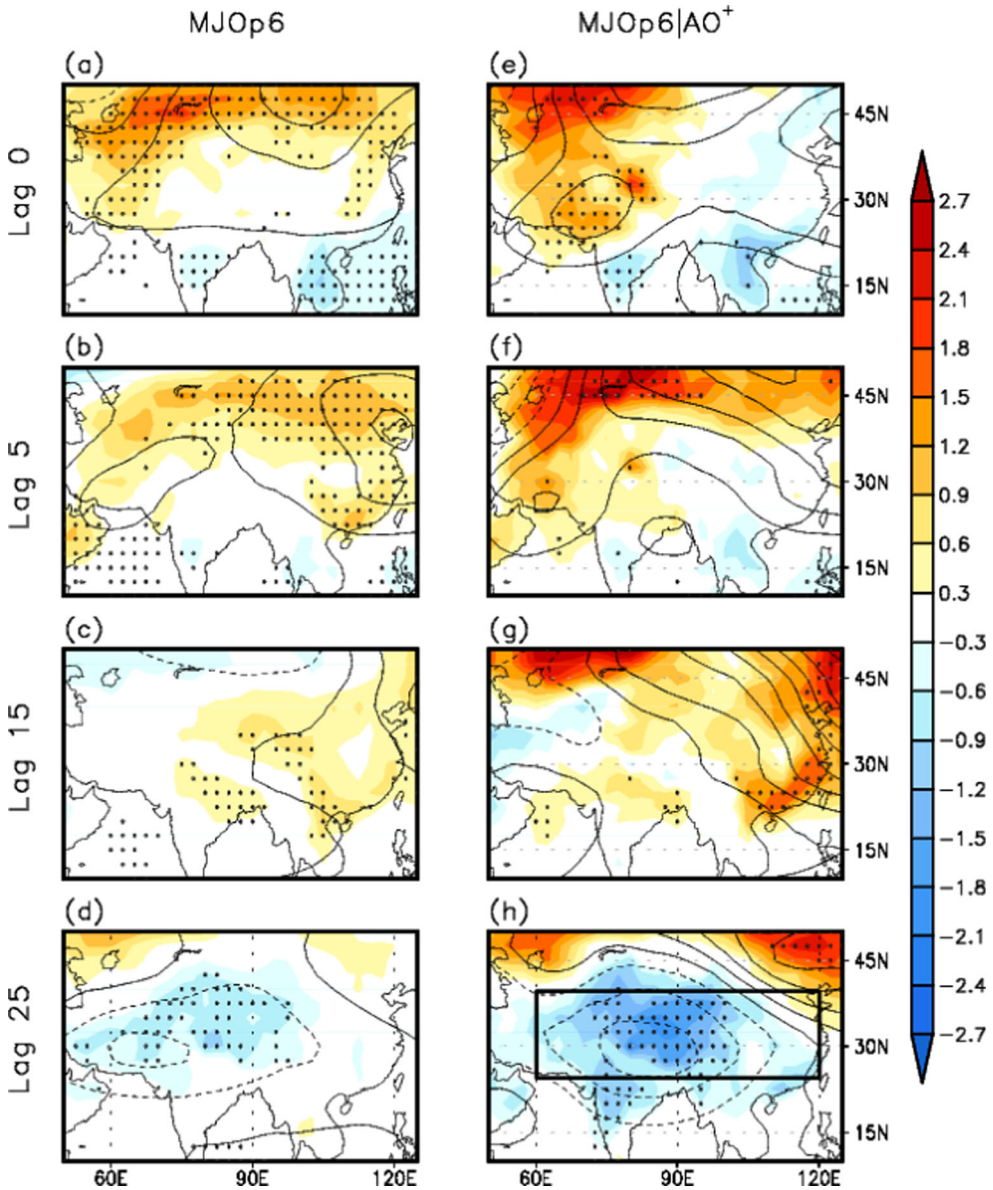

Fig. 6 As in Fig. 3 except for (**a**) − (**d**) the MJO phase 6 during all winters, and (**e**) − (**h**) the MJO phase 6 during AO^+ winter. Black box indicates the southern Asia region, [60° − 120°E, 25° − 45°N]. Note that the latitudinal domain is different from that in Fig. 3

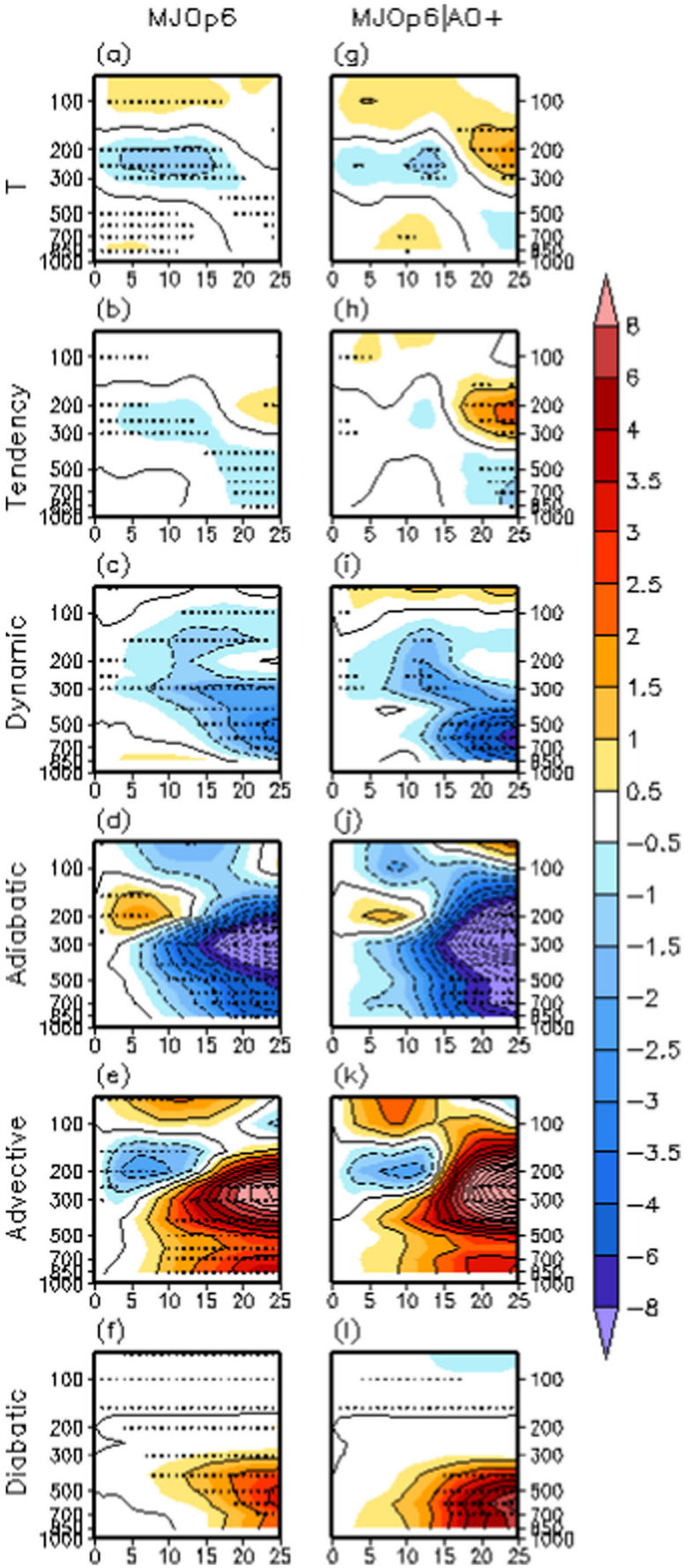
MJOp6
MJOp6|A0+
(a)
(g)
(b)
(h)
(c)
(i)
(d)
(j)
(e)
(k)
(f)
(l)
T
Tendency
Dynamic
Adiabatic
Advective
Diabatic
100
200
300
500
700
850
1000
0 5 10 15 20 25
8
6
4
3.5
3
2.5
2
1.5
1
0.5
−0.5
−1
−1.5
−2
−2.5
−3
−3.5
−4
−6
−8

◀ **Fig. 7** As in Fig. 4 except for (**a**) – (**f**) the MJO phase 6 during all winters, and (**g**) – (**l**) the MJO phase 6 during AO^+ winter for southern Asia

(Fig. 11a), the domain-averaged probability reaches ~5% in northern Asia at day 25; in particular, it is ~11% to the northeast of Baikal Lake. Over southern Asia, the probability amounts to ~7% with more than 11% over central China. In contrast, the probability rises remarkably up under the both AO states (Figs. 11b, c). During the negative AO (Fig. 11b), the domain-averaged probability is greater than 13% for northern Asia at day 25 with the northeast of Baikal Lake having more than 39%. The probability at day 25 under the positive AO (Fig. 11c) appears up to ~23.1% in central China and ~ 11.1% over southern Asia.

To examine the relative increase rate of this occurrence probability, the probability of cold temperature event is calculated for all days, which is estimated approximately 5% over Asia (not shown). Based on this, the percentage increase rate in the probability relative to 5% is plotted (thick contour in Figs. 10 and 11). The peak increase rate at the negative AO (Fig. 10a) is more than 90% over northern Asia and that for the positive AO (Fig. 10b) is more than 60% over southern Asia. The peak increase rate for the MJO composite of phase 2–3 is rather small, ~30% near southern Asia (Figs. 10c, d).

The peak percentage increase rate for the negative AO is more than six times the probability for all winter days at day 25 (Fig. 11b). This rate is ~2.5 times for the positive AO (Fig. 11c). The MJO only composite shows weaker relative increase (Fig. 11a). This result demonstrates that the mechanism responsible for the cold temperature anomaly also works well for the occurrence of extreme cold event. Interestingly, the occurrence probability doubles when both the MJO and AO are considered as compared to the case where only MJO is considered. Even if many previous studies have suggested that the sea-ice melting and loosened polar vortex are culprits of the extreme cold weather events (Tang et al. 2013; Gao et al. 2015; Sun et al. 2015), the tropical effect such as the MJO-induced teleconnection is also an important factor for driving or accentuating the extreme cold event. This study stresses that the incorporation of the two types of variability leads to the higher predictability of extreme cold event over Asia.

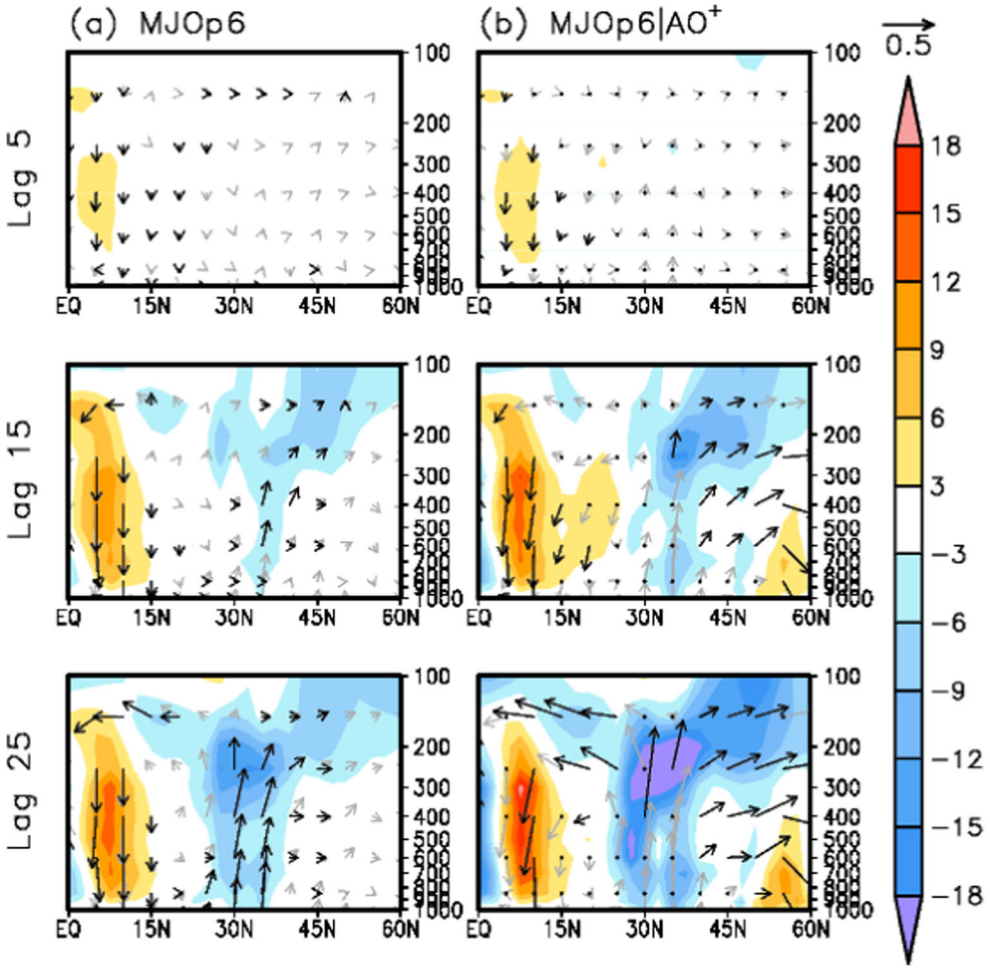

Fig. 8 Latitude-height cross section of lagged composite of temporally integrated adiabatic term related to the interaction between climatological temperature and vertical wind anomaly (shaded; K day) for (**a**) the MJO phase 6 during all winters and (**b**) the MJO phase 6 during AO^+ winter. Vector represents composite of temporally integrated meridional wind and pressure velocity. All fields are zonally averaged from 60° to 120°E. The reference wind vector (0.5) represents the magnitude of 50 m s^{-1} day for meridional wind and 0.2 Pa s^{-1} day for pressure velocity, respectively. Black vector represents statistically significant areas of the wind at the 95% confidence level

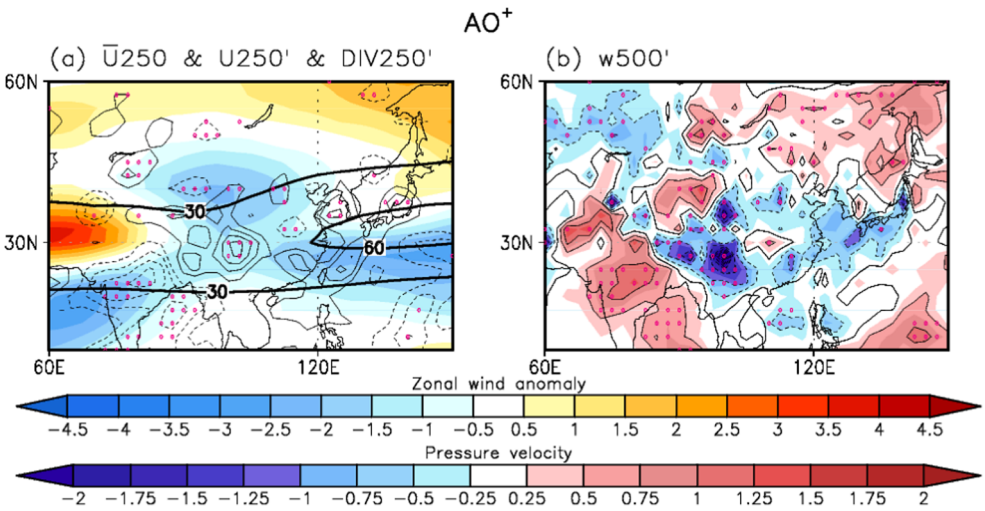

Fig. 9 **a** Composite map of climatological zonal wind (thick contour; intervals of 30 m s^{-1}), the zonal wind anomaly (shaded; m s^{-1}) and divergence anomaly (thin contour; intervals of 0.2×10^{-6} s^{-1}; the zero line is omitted) at 250 hPa for AO^+ winter. Dots indicate statistically significant areas of the divergence at the 90% confidence level. **b** Composite map of 500-hPa pressure velocity anomaly (units of 1.0^{-2} Pa s^{-1}) and dots represent the statistically significant areas at the 90% confidence level

6 Summary and Discussion

The MJO and AO are distinct two atmospheric modes and originate from the tropics and polar region, respectively. Both modes affect extreme weather and climate over Asia. The MJO produces the widespread cold anomaly over Asia at the phase 2–3, and the AO induces the cold anomaly over northern (southern) Asia at the negative (positive) phase. However, considering the combined effect, a more strengthened temperature variation appears. Under the negative AO state, a strong cold anomaly develops in northern Asia 20–25 days after the initial MJO phase 6 (which corresponds to the phase 2–3). The major contribution to the cold anomaly is the advection of the temperature anomaly by the climatological horizontal wind (Fig. 5b). The climatological northerly wind from Siberia, associated with the East Asia winter monsoon flow, advects the AO-induced cold air into northern Asia. On the other hand, under the positive AO state, the strong cold anomaly develops over southern Asia at day 25 and it is attributed to the adiabatic cooling due to the vertical wind anomaly (Fig. 8b). At the positive AO state, a weakening of the East Asia subtropical jet causes the upward motion at the jet entrance region to maintain thermal wind balance. Therefore, the ascent reinforces the adiabatic cooling which is already induced by the MJO-induced upward motion.

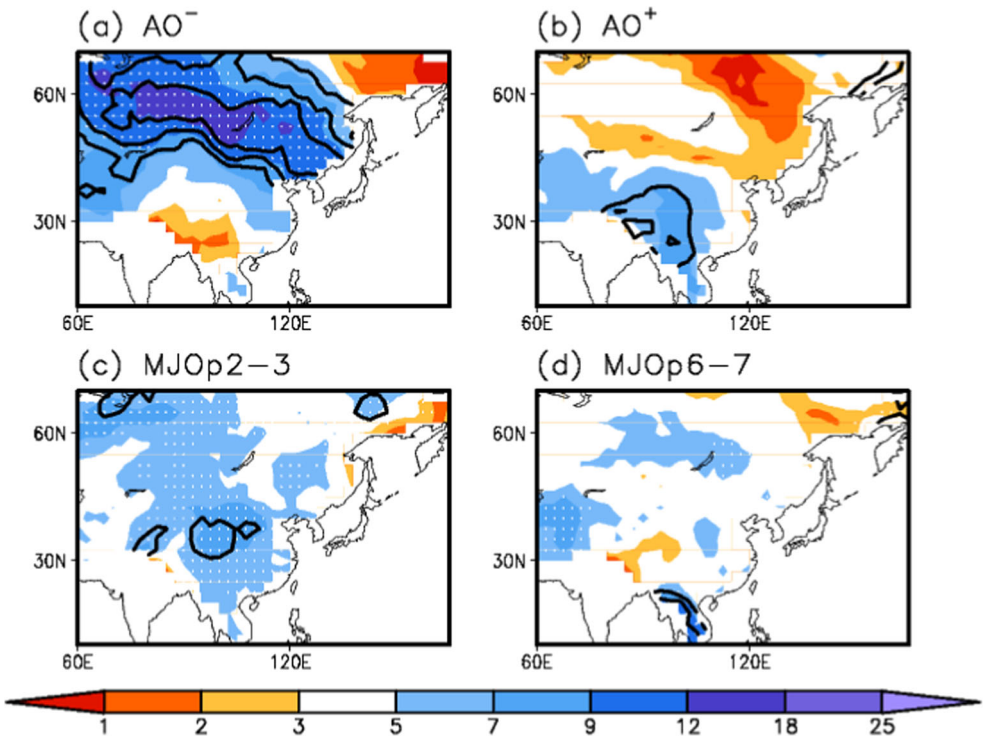

Fig. 10 The occurrence probability of extreme cold event (shaded) for (**a**) AO^- and (**b**) AO^+ winters, and (**c**) the MJO phase 2–3 and (**d**) phase 6–7. Dots represent significant areas at the 90% confidence level. The thick contour represents a percentage increase rate in the probability of extreme cold event compared to the occurrence probability for all winter days (intervals of 30, 60, and 90%)

Furthermore, the combined effect of the MJO and AO also influences on the occurrence probability of extreme cold event. Under the negative AO state, the occurrence probability of extreme cold event increases by more than 88% in northern Asia after 25 days of the initial phase 6 compared to that for all winter days. This increase accompanies a peak increase of six times the all winter days over the northeast of Baikal Lake. At the positive AO state, the percentage increase rate amounts to 51% for southern Asia with a peak increase rate which appears over central China and is 2.5 times the extreme cold event occurrence probability for all winter days. The extreme cold event occurrence probability for the combined consideration of the AO and MJO rises to be doubled as compared to that of the MJO impact only, suggesting that an incorporation of the MJO and AO helps improve the predictability of extreme cold event.

The AO undergoes variations on a variety of time scales including intraseasonal, interannual, and interdecadal time scales. Although this study focuses on the DJF-mean AO, previous studies have examined effects of month-to-month variability of the AO on winter temperature change over EA (e.g., Jeong and Ho 2005; Park et al. 2011). We repeated the same analysis but based on the monthly-mean AO index. The result is nearly identical to the present study (not shown). It is suggested that the processes analyzed above also operates on the monthly time scale.

This study suggests that the advection of the cold anomaly, which is from Siberia, due to the climatological wind and the adiabatic cooling, which is induced by the vertical wind anomaly, are the main causes of the extreme cold event over Asia. However, besides these processes, many other factors are responsible for the extreme cold event. For example, the cold surge can be caused by a sinking motion upstream of the upper-tropospheric trough as cold air is vertically advected from a higher level to the surface (Wu and Chan 1997); and cold advection by northerly flow due to a westward expansion of the Aleutian low (Jhun and Lee 2004) induces a cold surge event. Additionally, a passage of the upper-tropospheric wave train can deepen preexisting trough and this can induce a transient cold surge event (Watanabe 2004; Takaya and Nakamura 2005). Note that, however, in this study, this type of transient synoptic-scale disturbance effects is absent

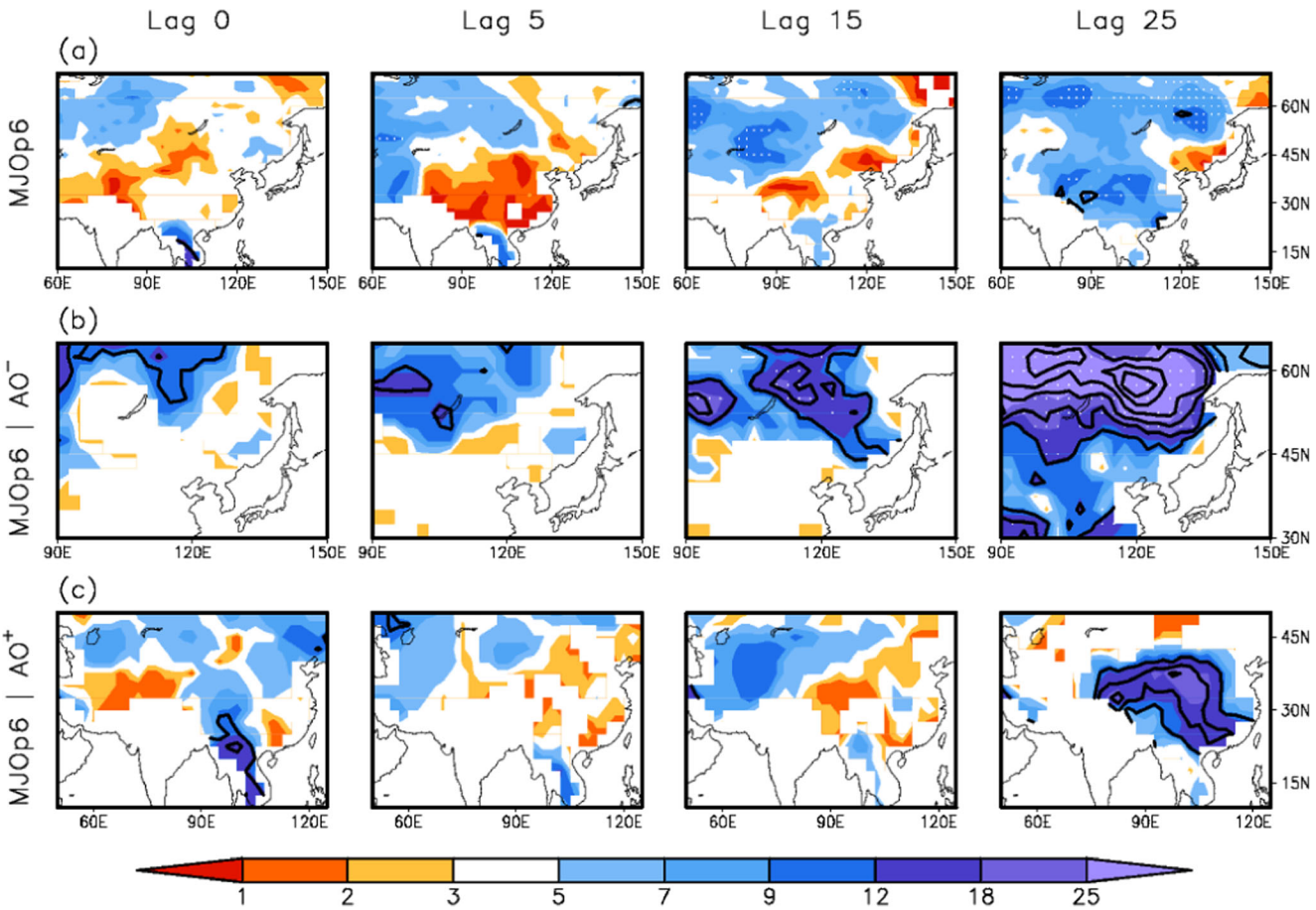

Fig. 11 As in Fig. 10, but for the MJO phase 6 during (**a**) all, (**b**) AO^-, and (**c**) AO^+ winters at lagged 0, 5, 15, and 25 days. Dots indicate statistically significant areas at the 90% confidence level. A percentage increase rate of the occurrence probability compared to the occurrence probability for all winter days (thick contour) has intervals of 100, 200, 300, 400, 500, and 600%. Note that the latitudinal domains are different for (a), (b) and (c)

because the day-to-day variability of the disturbances is canceled out by using the DJF-mean AO index.

In this study, a combination of the MJO and AO effects is examined. However, in fact, more complicated nonlinear processes exist in the combined influences, because the MJO and AO interact and feedback each other (Zhou and Miller 2005; Flatau and Kim 2013). The MJO modulates the polar vortex and therefore the AO (L'Heureux and Higgins 2008; Garfinkel et al. 2012), while a background state related to the AO (or North Atlantic oscillation which has a high correlation with the AO) can modify the MJO-related tropical convection (Lin and Brunet 2011; Gong et al. 2014). Furthermore, it is obvious that the pattern of teleconnection in response to the MJO may be changed depending on the AO state. A further study is needed to investigate the feedback process.

Previous studies have suggested that the AO (or Northern annular mode, NAM) can be modulated by the ENSO (Quadrelli and Wallace 2002; Garfinkel and Hartmann 2008; L'Heureux et al. 2017). However, the correlation coefficient between the DJF-mean AO and Nino 3.4 (from http://www.cpc.ncep.noaa.gov/data/indices/ersst5.nino.mth.81-10.ascii) indices calculated is about −0.12, implying that the dependence of the AO and ENSO is insignificant. However, the relationship between the AO and ENSO has strengthened after the mid-1990s (Li et al. 2014). Hence, it is needed to explore the dependence of the AO on the ENSO in detail and whether the strengthened relationship can modify temperature variations over Asia.

Acknowledgements This work was supported by the National Research Foundation of Korea (NRF) grant funded by the Korea government (MSIP) (No. NRF-2018R1A2A2A05018426) and the KMA Research and Development Program under Grant KMI 2018–01012. We would like to thank the two anonymous reviewers for their careful and helpful comments and suggestions.

References

Adames, Á.F., Wallace, J.M.: Three-dimensional structure and evolution of the MJO and its relation to the mean flow. J. Atmos. Sci. **71**, 2007–2026 (2014). https://doi.org/10.1175/JAS-D-13-0254.1

Bessafi, M., Wheeler, M.C.: Modulation of South Indian Ocean tropical cyclones by the madden–Julian oscillation and convectively coupled equatorial waves. Mon. Weather Rev. **134**, 638–656 (2006)

Branstator, G.: Circumglobal teleconnections, the Jetstream waveguide, and the North Atlantic oscillation. J. Clim. **15**, 1893–1910 (2002)

Flatau, M., Kim, Y.-J.: Interaction between the MJO and polar circulations. J. Clim. **26**, 3562–3574 (2013). https://doi.org/10.1175/JCLI-D-11-00508.1

Gao, Y., Coauthors: Arctic Sea ice and Eurasian climate: a review. Adv. Atmos. Sci. **32**, 92–114 (2015). https://doi.org/10.1007/s00376-014-0009-6

Garfinkel, C.I., Hartmann, D.L.: Different ENSO teleconnections and their effects on the stratospheric polar vortex. J. Geophys. Res. **113**, D18114 (2008). https://doi.org/10.1029/2008JD009920.

Garfinkel, C.I., Feldstein, S.B., Waugh, D.W., Yoo, C., Lee, S.: Observed connection between stratospheric sudden warmings and the madden-Julian oscillation. Geophys. Res. Lett. **39**, L18807 (2012). https://doi.org/10.1029/2012GL053144

Gong, D.Y., Gao, Y., Guo, D., Mao, R., Yang, J., Hu, M., Gao, M.: Interannual linkage between Arctic/North Atlantic oscillation and tropical Indian Ocean precipitation during boreal winter. Clim. Dyn. **42**(3–4), 1007–1027 (2014)

Hall, J.D., Matthews, A.J., Karoly, D.J.: The modulation of tropical cyclone activity in the Australian region by the madden–Julian oscillation. Mon. Weather Rev. **129**, 2970–2982 (2001)

Hendon, H.H., Liebmann, B.: The intraseasonal (30-50 day) oscillation of the Australian summer monsoon. J. Atmos. Sci. **47**, 2909–2923 (1990)

Holton, J.R.: An Introduction to Dynamic Meteorology, 4th edn. Elsevier Academic Press (2004) 167 pp

Hoyos, C.D., Webster, P.J.: The role of intraseasonal variability in the nature of Asian monsoon precipitation. J. Clim. **20**, 4402–4424 (2007)

Jeong, J.-H., Ho, C.-H.: Changes in occurrence of cold surges over East Asia in association with Arctic oscillation. Geophys. Res. Lett. **32**, L14704 (2005). https://doi.org/10.1029/2005GL023024

Jeong, J.-H., Ho, C.-H., Kim, B.-M., Kwon, W.-T.: Influence of the madden-Julian oscillation on wintertime surface air temperature and cold surges in East Asia. J. Geophys. Res. **110**, D11104 (2005). https://doi.org/10.1029/2004JD005408.

Jeong, J.-H., Kim, B.-M., Ho, C.-H., Noh, Y.-H.: Systematic variation in wintertime precipitation in East Asia by MJO-induced extratropical vertical motion. J. Clim. **21**, 788–801 (2008)

Jhun, J.-G., Lee, E.-J.: A new east Asian winter monsoon index and associated characteristics of winter monsoon. J. Clim. **17**, 711–726 (2004)

Kim, H.-K., Seo, K.-H.: Cluster analysis of tropical cyclone tracks over the western North Pacific using a self-organizing map. J. Clim. **29**, 3731–3751 (2016)

Kobayashi, S., Ota, Y., Harada, Y., Ebita, A., Moriya, M., Onoda, H., Onogi, K., Kamahori, H., Kobayashi, C., Endo, H., Miyaoka, K., Takahashi, K.: The JRA-55 reanalysis: general specifications and basic characteristics. J. meteor. Soc. Japan. **93**, 5–48 (2015). https://doi.org/10.2151/jmsj.2015-001

L'Heureux, M.L., Coauthors: Strong relations between ENSO and the Arctic oscillation in the north American multimodel ensemble. Geophys. Res. Lett. **44**, 11,654–11,662 (2017). https://doi.org/10.1002/2017GL074854

L'Heureux, M.L., Higgins, R.W.: Boreal winter links between the madden-Julian oscillation and the Arctic oscillation. J. Clim. **21**, 3040–3050 (2008)

Li, F., Wang, H.J., Liu, J.P.: The strengthening relationship between Arctic oscillation and ENSO after the mid-1990s. Int. J. Climatol. **34**, 2515–2521 (2014)

Lin, H., Brunet, G.: The influence of the madden–Julian oscillation on Canadian wintertime surface air temperature. Mon. Weather Rev. **137**, 2250–2262 (2009)

Lin, H., Brunet, G.: Impact of the North Atlantic oscillation on the forecast skill of the madden-Julian oscillation. Geophys. Res. Lett. **38**, L02802 (2011). https://doi.org/10.1029/2010GL046131

Lin, H., Brunet, G., Mo, R.: Impact of the madden–Julian oscillation on wintertime precipitation in Canada. Mon. Weather Rev. **138**, 3822–3839 (2010)

Liu, C., Tian, B., Li, K.-F., Manney, G.L., Livesey, N.J., Yung, Y.L., Waliser, D.E.: Northern hemisphere mid-winter vortex-displacement and vortex-split stratospheric sudden warmings: influence of the madden-Julian oscillation and quasi-biennial oscillation. J. Geophys. Res. Atmos. **119**, 12,599–12,620 (2014). https://doi.org/10.1002/2014JD021876

Madden, R.A., Julian, P.R.: Description of global-scale circulation cells in the tropics with a 40–50 day period. J. Atmos. Sci. **29**, 1109–1123 (1972)

Marshall, A.G., Hendon, H.H., Son, S.-W., Lim, Y.: Impact of the quasi-biennial oscillation on predictability of the madden–Julian oscillation. Clim. Dyn. **49**, 1365–1377 (2017). https://doi.org/10.1007/s00382-016-3392-0

Moon, J.-Y., Wang, B., Ha, K.-J.: ENSO regulation of MJO teleconnection. Clim. Dyn. **37**, 1133–1149 (2011)

Park, T.-W., Ho, C.-H., Yang, S., Jeong, J.-H.: Influences of Arctic oscillation and madden-Julian oscillation on cold surges and heavy snowfalls over Korea: a case study for the winter of 2009–2010. J. Geophys. Res. **115**, D23122 (2010). https://doi.org/10.1029/2010JD014794

Park, T.-W., Ho, C.-H., Yang, S.: Relationship between the Arctic oscillation and cold surges over East Asia. J. Clim. **24**, 68–83 (2011)

Quadrelli, R., Wallace, J.M.: Dependence of the structure of the northern hemisphere annular mode on the polarity of ENSO. Geophys. Res. Lett. **29**, 2132–47-4 (2002). https://doi.org/10.1029/2002GL015807.

Seo, K.-H., Lee, H.-J.: Mechanisms for a PNA-like teleconnection pattern in response to MJO. J. Atmos. Sci. **74**, 1767–1781 (2017). https://doi.org/10.1175/JAS-D-16-0343.1

Seo, K.-H., Son, S.-W.: The global atmospheric circulation response to tropical diabatic heating associated with the madden–Julian oscillation during northern winter. J. Atmos. Sci. **69**, 79–96 (2012)

Seo, K.-H., Lee, H.-J., Frierson, D.M.W.: Unraveling the teleconnection mechanisms that induce wintertime temperature anomalies over the northern hemisphere continents in response to the MJO. J. Atmos. Sci. **73**, 3557–3571 (2016)

Shimizu, M.H., Ambrizzi, T.: MJO influence on ENSO effects in precipitation and temperature over South America. Theor. Appl. Climatol. **124**(1–2), 291–301 (2016). https://doi.org/10.1007/s00704-015-1421-2

Sun, L., Deser, C., Tomas, R.A.: Mechanisms of stratospheric and tropospheric circulation response to projected Arctic Sea ice loss. J. Clim. **28**, 7824–7845 (2015). https://doi.org/10.1175/JCLI-D-15-0169.1

Takaya, K., Nakamura, H.: Mechanisms of intraseasonal amplification of the cold Siberian high. J. Atmos. Sci. **62**, 4423–4440 (2005). https://doi.org/10.1175/JAS3629.1

Tang, Q., Zhang, X., Yang, X., Francis, J.A.: Cold winter extremes in northern continents linked to arctic sea ice loss. Environ. Res. Lett. **8**, 014036 (2013). https://doi.org/10.1088/1748-9326/8/1/014036

Thompson, D.W.J., Wallace, J.M.: The Arctic oscillation signature in the wintertime geopotential height and temperature fields. Geophys. Res. Lett. **25**, 1297–1300 (1998). https://doi.org/10.1029/98GL00950

Vecchi, G.A., Bond, N.A.: The madden-Julian oscillation (MJO) and northern high latitude wintertime surface air temperatures. Geophys. Res. Lett. **31**, L04104 (2004). https://doi.org/10.1029/2003GL018645

Watanabe, M.: Asian jet waveguide and a downstream extension of the North Atlantic oscillation. J. Clim. **17**, 4674–4691 (2004). https://doi.org/10.1175/JCLI-3228.1

Wheeler, M.C., Hendon, H.H.: An all-season real-time multivariate MJO index: development of an index for monitoring and prediction. Mon. Weather Rev. **132**, 1917–1932 (2004)

Wu, M.C., Chan, J.C.L.: Upper-level features associated with winter monsoon surges over South China. Mon. Weather Rev. **125**, 317–340 (1997)

Yoo, C., Lee, S., Feldstein, S.: Mechanisms of Arctic surface air temperature change in response to the madden-Julian oscillation. J. Clim. **25**, 5777–5790 (2012)

Zhou, S., Miller, A.J.: The interaction of the madden-Julian oscillation and the Arctic oscillation. J. Clim. **18**, 143–159 (2005)

Zhou, S., L'Heureux, M., Weaver, S., Kumar, A.: A composite study of the MJO influence on the surface air temperature and precipitation over the continental United States. Clim. Dyn. **38**, 1458–1471 (2012)